Nigerian Journal of Physics (NJP)
ISSN online: 3027-0936
ISSN print: 1595-0611
DOI: https://doi.org/10.62292/njp.v34i2.2025.444
Volume 34(2), June 2025

Band-gap, Urbach's energy tail and Magnetic Analysis of Cs^{3+}-Ni^{2+} Doped Zinc Spinel Ferrites Nanoparticles

[1]Ibrahim, U. M., [1,2]Maikudi, S., *[1]Musa, A., [3]Mohammed, J. and [1]Ahmed, F.

[1]Department of Physics, College of Physical Science, Bayero University Kano, Kano State, Nigeria.
[2]Department of Science Laboratory Technology, College of Science and Technology Hussaini Adamu Federal Polytechnic Kazaure, Jigawa State, Nigeria.
[3]Department of Physics, Faculty of Science, Federal University Dutse, Jigawa State, Nigeria.

*Corresponding author's email: amusa.phy@buk.edu.ng

Keywords:
Band gap energy, Coercivity, Magnetization, Rare-earth element, Urbach energy, Zinc spinel ferrite.

ABSTRACT

Over the years, spinel ferrites has attracted the attention of the research community as a result of the possibility for a variety of applications. Several attempts have been made in order to modify the optical and magnetic properties of spinel ferrites. Cs^{3+}–Ni^{2+} substituted zinc spinel ferrite with chemical composition $Zn_{1-x}Cs_xFe_{2-x}Ni_xO_4$ (x=0.0, 0.1, 0.2) was prepared using sol-gel auto-combustion method and calcinated at 700°C for 5hrs. The UV-vis spectroscopy shows the presence of UV-cut-off at 447nm. The urbach energy tail increase with increase in Cs^{3+} and Ni^{2+} ions concentration. The band gap energy of the prepared samples was found to be in a semiconductor region. VSM analysis shows the appearance of super-exchange interaction as a result of replacement of Zn^{2+} by Cs^{3+} ions in A-site and Fe^{3+} by Ni^{2+} ions in B-site resulted in the slight decrease in the values of M_s and H_c. The values of R is less than 0.5 which shows a single magnetic domain with uniaxial anisotropy. The values of K and H_k decrease with addition of Cs^{3+} and Ni^{2+} ions concentration. This decrease shows the anisotropic nature of the prepared samples.

INTRODUCTION

Over the years, spinel ferrites has attracted the attention of the research community as a result of the possibility for a variety of applications (Kadam *et al*., 2020). The crystal structure of spinel ferrites is such that each cubic unit cell of a spinel ferrites contains eight formula units with fifty six ions. Thus, there are thirty two oxygen anions, eight divalent metal cations and sixteen trivalent ferric cations. Large size of oxygen ions, form a closely packed face-centered cubic structure (fcc) with smaller M^{2+} cations occupying the interstitial position as reported by the ferrites researchers (Narang & Pubby, 2021, Debnath & Das, 2020). Moreover, there are two types of crystallographic sites present in the spinel structure. Namely the B-site (octahedral) which is surrounded by six oxygen ions and A-site (tetrahedral) which is surrounded by four oxygen ions. Thus in each spinel unit cell, there are sixteen octahedral and eight tetrahedral sites present (Debnath *et al*., 2021, Azhar *et al*., 2020).

Many attempt have been made in order to modify the optical and magnetic properties of spinel ferrites. Pubby *et al* (2020) employed pechins sol-gel method and synthesized nickel-cobalt spinel ferrites with chemical composition $Ni_{1-x}Co_xFe_2O_4$ to investigate its magnetic, elastic, dielectric, microwave absorption and optical properties. It was observed that saturation magnetization, coercivity and Curie temperature increased with increase in the amount of cobalt doping. The lower coercivity (694.7Oe) and optimized combination of high Ms (86.12emug^{-1}) was achieved in composition NC 0.90 which suggest its possibility to be use in recording media applications (Pubby *et al*., 2020). Manikandan *et al* (2014) synthesized Co^{2+} doped zinc spinel ferrite via microwave combustion method to study its structural, optical and magnetic properties. The photoluminescence spectra (PL) and UV-visible diffuse reflectance spectra (DRS) revealed that the broad band visible emission was observed in the entire PL spectrum and the energy band gap estimated is about 2.1eV. The VSM analysis revealed the variations of saturation magnetization as higher and lower composition. The higher composition of the prepared samples (0.3, 0.4, and 0.5) shows ferromagnetic behavior while the low composition of the prepared samples (0.0, 0.1 and 0.2) shows super paramagnetic behavior and the Ms increased with addition of Co^{2+} ion concentration to attained the highest value of 65.20emu/g

(Manikandan *et al*., 2014, Kareemah *et al*. 2024). Niaz *et al* (2021) employed one step sol-gel self-ignition approach and synthesized rare-earth doped spinel ferrite with chemical composition $Ni_{0.5}Zn_{0.5}Fe_{2-x}Yb_xGd_xO_4$ (x=0.0, 0.2, 0.4, 0.6, 0.8 and 1.0) to study its structural, conductive and magneto-optical properties. It was observed that the saturation magnetization, remanence magnetization and coercivity values are respectively in the range of 12.76emu/g to 39.36emu/g, 9.23emu/g to 28.22emu/g and 290.5Oe to 347.9Oe. The range of the optical band gap were found to be in a semiconductor region (2.04eV to 2.28eV). The electrical conductivity of the prepared samples indicate the semiconducting trend with the rise of temperature from 323k to 563k. Band gap energy in a semiconductor region and improved electrical conductivity at higher temperature make the prepared samples prominent candidate for nanoantennas, quantum information, sensing application, isolators, modulators, data storage devices and energy storage devices (Niaz *et al*., 2021).

After careful review of literatures, sol gel auto combustion method was used to synthesized Cs^{3+}–Ni^{2+} substituted zinc spinel ferrite. Sol gel auto combustion offers variety of advantages over other methods such as solid state reaction method and co-precipitation method. The advantages include simplicity of the method, low time for the reaction to take place, homogeneity of the particles, good control of the stoichiometry as a result of molecular-level mixing, the utilization of cost-effective chemicals and required low calcination temperature to produce the final product (Mohammed *et al*., 2021).

MATERIALS AND METHODS

Experimental Procedure

Synthesis and characterization method

Sol-gel auto-combustion technique was employed to synthesize the desired spinel ferrites. The details of the experiment can be found in our previous paper (Maikudi *et al*., 2023). Briefly, AR grade chemicals were used to synthesize $Zn_{1-x}Cs_xFe_{2-x}Ni_xO_4$ (x=0.0, 0.1, 0.2) using sol-gel auto-combustion technique. To study the optical properties of the prepared samples, UV-vis-NIR spectrophotometer (Varian, Cary 5000) were used in 175-3300nm spectral range. Vibrating sample magnetometer (Lakeshore 7410) was employed to determine the M-H hysteresis loop and use it to study the magnetic properties of the prepared samples

RESULTS AND DISCUSSION

Optical Analysis

The incident visible and UV radiation gives energy to the non-bonding electrons and consequently interact with the anti-bonding molecules in the prepared sample thereby giving the UV absorption spectra which could be to evaluate the optical properties of the prepared samples. Figure. 1 presents the variation of absorbance against wavelength of $Zn_{1-x}Cs_xFe_{2-x}Ni_xO_4$ (x=0.0, 0.1, 0.2) at the range of 200–800. The prepared samples were found to strongly absorb UV light as evident in the absorbance spectra, similar scenario was reported by Rahman *et al*. (2021). The spectra show absorption peak at 290 nm (i.e. hyperchromic effect as a result of $\pi - \pi^*$ transition) and two reflection peaks at 461 and 682 nm (i.e. hypochromic effect as a result of $n - \pi^*$ transition) in all the samples. In addition, two absorption peaks were observed at 725 and 765 nm (i.e. hyperchromic effect as a result of $\pi - \pi^*$ transition) for the sample with x=0.02. The reflection peak at 461 nm disappears when the concentration of Cs^{3+}–Ni^{2+} was increased from x=0.1 to x=0.2. Similarly, the reflection peak at 682 nm also disappears, but we may assume that this reflection peak was converted to absorption peak (725 nm) and shift to higher wavelength. From the foregoing discussion, we could infer that the substitution of Cs^{3+}–Ni^{2+} enhances the absorption of the incident light. The bandgap (E_g) of the prepared samples was determined from Kubelka–Munk relation.

$$(\alpha h\upsilon)^n = K(h\upsilon - E_g) \quad (1)$$

where α is the absorption coefficient, h is Planck's constant ($6.6260 \times 10^{-34}\ J.s$); υ is the frequency of the incident photon; and n is a constant whose values may be 1/2 (signifying allowed direct transition), 2 (signifying allowed indirect transition), 3/2 (signifying forbidden direct transition), and 3 (signifying forbidden indirect transition). The plot of $(\alpha h\upsilon)^2$ against E_g for $Zn_{1-x}Cs_xFe_{2-x}Ni_xO_4$ (x=0.0, 0.1, 0.2) is presented in Figure 2. The values of E_g is determined by linear extrapolation of the plot up to the point where $\alpha = 0$ (i.e. where it cut the *x*-axis). The values of the E_g of the prepared samples for x=0.0, x=0.1 and x=0.2 were respectively found to be 1.64, 1.77 and 1.88 eV (Table 1). Clearly the values of E_g shows an increase with addition of Cs^{3+}–Ni^{2+} content. There could be several reasons attached to the observation of the increase in values of E_g. For instance, when electrons are tightly bonded to the nucleus of the atom, a large amount of energy (i.e. E_g) will be needed to remove the electrons from the atom (Aslam *et al*., 2020). This shows that increase in the concentration of Cs^{3+}–Ni^{2+} resulted in increased need for energy (i.e. E_g). Additionally, factors such as quantum confinement and size of the crystallite could influence the values of the E_g (Alrebdi *et al*., 2022).

In the energy range just below the edge of the band, the values of α produced a minute temperature-dependent exponential tail in accordance with the Urbach energy law based on Equation (2)

$$\alpha = \alpha_0 exp\left(\frac{h\upsilon}{E_U}\right) \quad (2)$$

Where α_0 represents the characteristic parameter of the material, $h\upsilon$ represents the energy of the incident radiation, and E_U represents the Urbach energy which can be obtained through taking the log of both sides of

Equation 2 thereby modifying it to a linear graph equation

$$\alpha = \left(\frac{1}{E_U}\right) h\nu\alpha_0 . \quad (3)$$

The E_U values of the samples were determined via linear fitting of the plot of $ln\ ln\ \alpha$ against $h\nu$, and taking the reciprocal of the slope. The values of the E_U for x=0.0, x=0.1 and x=0.2 were respectively found to be 3.06, 3.42 and 4.38 meV as presented in Table 1. The appearance of E_U is a clear indication of disorder in the crystalline structure as a result of the substitution of Cs^{3+}–Ni^{2+} which causes the bonds of localized electrons to broaden (Ananth Kumar *et al*., 2014). The values of E_U tend to increase with increase in Cs^{3+}–Ni^{2+} concentration, this expected as the more the Cs^{3+}–Ni^{2+} are incorporated in the crystal structure of the prepared samples, the more the structural distortion that may occur.

Table 1: Urbach's energy and band gap energy of $Zn_{1-x}Cs_xFe_{2-x}Ni_xO_4$ (x=0.0, 0.1, 0.2)

X	Urbach's energy (meV)	Band gap (eV)
0.0	3.06	1.64
0.1	3.42	1.77
0.2	4.38	1.88

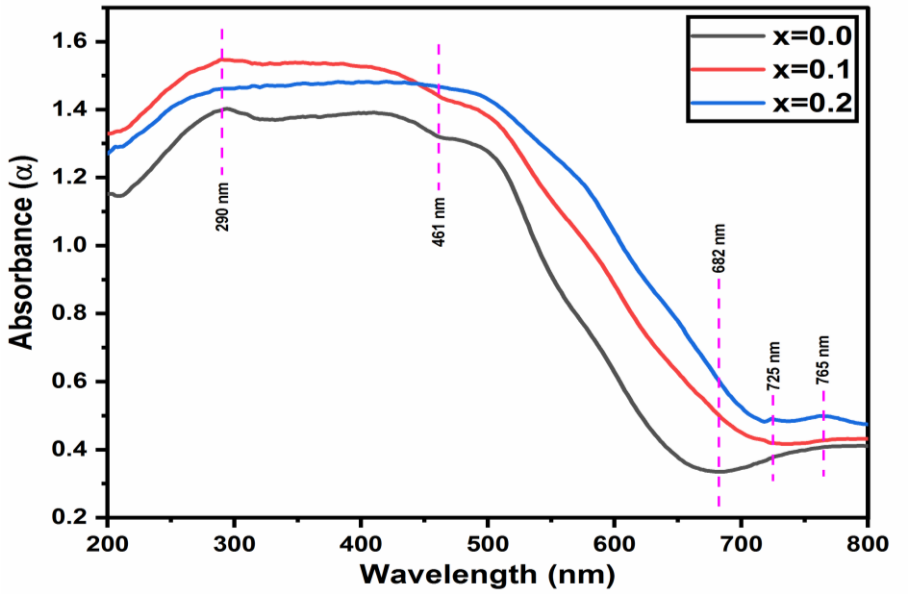

Figure 1: Absorbance of $Zn_{1-x}Cs_xFe_{2-x}Ni_xO_4$ (x=0.0, 0.1, 0.2)

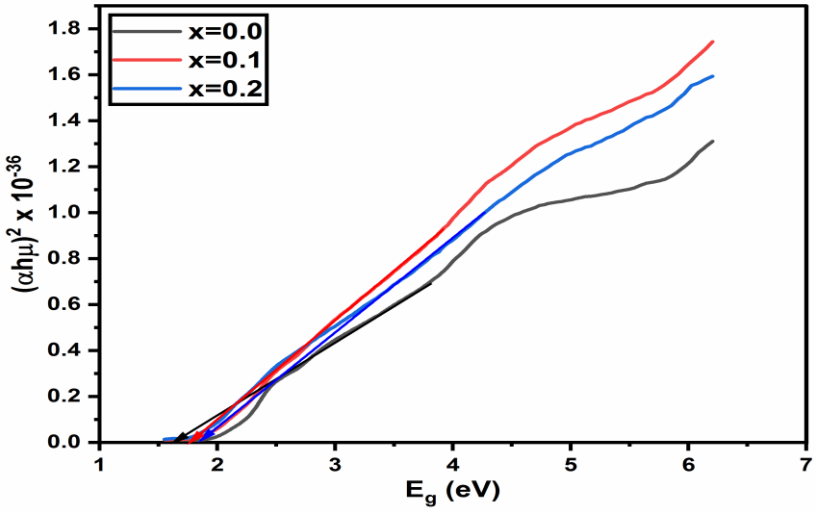

Figure 2: Band gap of $Zn_{1-x}Cs_xFe_{2-x}Ni_xO_4$ (x=0.0, 0.1, 0.2)

VSM Analysis

Figure 3 present M–H hysteresis loop $Zn_{1-x}Cs_xFe_{2-x}Ni_xO_4$ (x=0.0, 0.1, 0.2). Various magnetic parameters such as saturation magnetization (M_s), remnant magnetization (M_r) and coercivity (H_c) were determined from the M–H hysteresis loops. It was observed that the M_s values are 40.86emu/g, 34.12emu/g and 32.08emu/g for x=0.0, x=0.1 and x=0.2 respectively. The decreasing trend of the M_s values could be attributed to the higher magnetic moment of Fe^{3+} ion compared to Ni^{2+} ion residing in B-site (Puli *et al*., 2015). The M_s values observed are in good agreement with the values reported in literature (Sandeep *et al*., 2022; Almessiere *et al*., 2022; and Niaz *et al*., 2021). In addition, magnetic exchange interaction at A-and B-sites, cations disorder and canted spin moments on the surface of the nanoparticles have notable effect on the M_s values (Akhtar *et al*., 2020). The M_r values were found to be 12.21emu/g, 13.94emu/g and 14..01emu/g for x=0.0, x=0.1 and x=0.2 respectively. Larger ionic radius of Cs^{3+} ion compared to Zn^{2+} ion in A-site and Ni ion compared to Fe ion in B-site could be the possible reason of this increase (Puli *et al*., 2015; and Naik *et al*., 2013). The H_c values decrease with increase in Cs – Ni content as listed in Table 2. The observed H_c values are in good agreement with earlier reported literature by Almessiere *et al* (2022) and Niaz *et al* (2021).

In addition to M_s, M_r and H_c observed from the M–H hysteresis loops, magnetic parameters such as remanence ratio (R), magnetic moment (n_B), anisotropy constant (K), anisotropy field (H_k) and initial permeability (μ_i) were respectively calculated using Equation (4), Equation (5), Equation (6), Equation. (7) and Equation (8).

$$R = \frac{M_r}{M_s} \quad (4)$$

$$n_B = \frac{M_w \, x \, M_s}{5585} \; (\mu_B) \quad (5)$$

$$K = \frac{H_c \, x \, M_s}{0.96} \quad (6)$$

$$H_k = \frac{2K}{\mu_o \, x \, M_s} \quad (7)$$

$$\mu_i = \frac{M_s^2 \, x \, D}{K} \quad (8)$$

Where M_w is a molecular weight of the prepared sample, μ_O is a permittivity of free space which has the value of $4\pi \, x \, 10^{-7} H/M$, μ_B is a unit of magnetic moment which can be written as Bohr magneton (BM) and D is a crystallite size of the prepared samples (Hamza *et al*., 2022, Kiran *et al*., 2021, Ghorbani *et al*., 2022). It was observed from Table 2 that the lower the coercive field, the lower the magnetic anisotropy in the prepared samples. Hence the decreasing trend of H_c could be attributed to the magnetic anisotropy (Zan *et al*., 2013). The remanence ratio (R) is a measure of exchange interaction and magnetor-crystalline anisotropy. The R values were found to be 0.25, 0.41 and 0.44 for x=0.0, x=0.1 and x=0.2 respectively. According to Stoner-Wohlfarth's ($S-W$) theory, the values observed are less than 0.5 which indicate that the prepared samples has a single magnetic domain with uniaxial anisotropy (Ghorbani *et al*., 2022). The variation of M_s, M_r, H_c and R with addition of Cs^{3+}–Ni^{2+} content was presented in Figure 4. It was also observed from Table 2 that the values of the net magnetic moment (n_B) decrease from $2.11\mu_B$ to $1.47\mu_B$ with addition of Cs^{3+}–Ni^{2+} content, similar result was reported by Sandeep A. et al (Sandeep *et al*., 2022). This decrease could be attributed to the lowering difference of magnetic moment A and B-sites as well as lowering of A-B super exchange interactions. Usually, the magnetic moment of doped spinel ferrites emerge due to exchange interaction between the metal cations preset at A- and B-sites (A-B super exchange interaction) (Hamza *et al*., 2022. Toprak, 2014, Nasir et al., 2013). Moreover, both anisotropic constant and anisotropic field decrease with increase in Cs^{3+}–Ni^{2+} content as observed from Table 2. The decreasing trend of these values justified that the prepared samples has anisotropic nature and softer to magnetize in the direction of easy axis (Hamza *et al*., 2022). No considerable contribution to the magnetic properties is expected from $CsFeO_3$ phase due to the fact that is a canted antiferromagnetic with a feeble magnetization and Neel temperature of 674k (Shah & Kotnala, 2012).

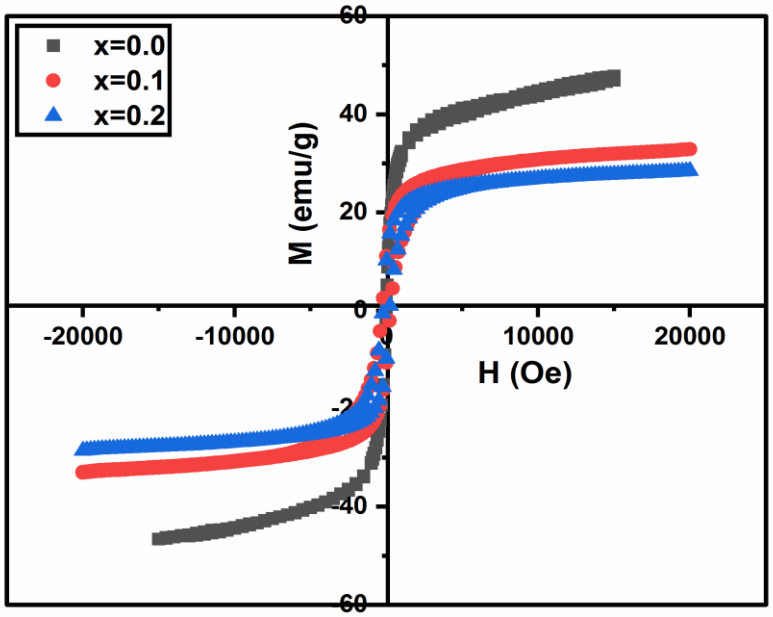

Figure 3: M-H hysteresis loop of $Zn_{1-x}Cs_xFe_{2-x}Ni_xO_4$ (x=0.0, 0.1, 0.2)

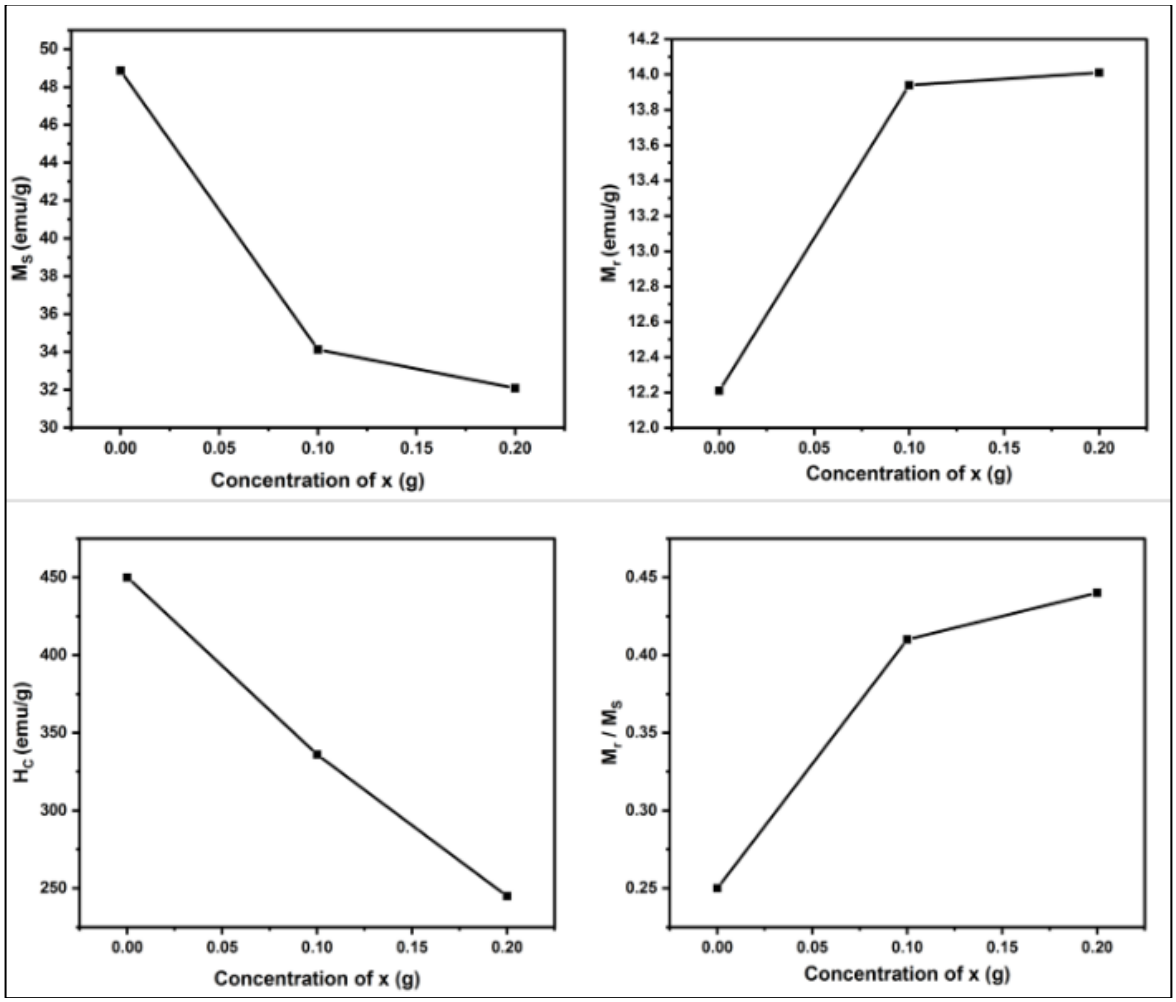

Figure 4 Variation of Ms, Mr, Hc and R for $Zn_{1-x}Cs_xFe_{2-x}Ni_xO_4$ (x=0.0, 0.1, 0.2)

Table 2: Magnetic parameters of $Zn_{1-x}Cs_xFe_{2-x}Ni_xO_4$ (x=0.0, 0.1, 0.2)

X	MW (g/mol)	Ms (emu/g)	Mr (emu/g)	Hc (Oe)	Mr/Ms	n_B (μ_B)	K (ergg-1)	H_k x10^7	μ_i
0.0	241.07	48.86	12.21	449.99	0.25	2.11	22902	74	8.56
0.1	248.10	34.12	13.94	336.07	0.41	1.52	11944	55	8.51
0.2	255.14	32.08	14.01	244.93	0.44	1.47	8184	40	5.38

CONCLUSION

Cs^{3+} - Ni^{2+} substituted zinc spinel ferrite with chemical composition $Zn_{1-x}Cs_xFe_{2-x}Ni_xO_4$ (x=0.0, 0.1, 0.2) were synthesized successfully via sol-gel Auto-combustion method. From the analysis of the data obtained, the following conclusions: according to the optical study, a UV-cut-off was observed at 447nm. This cut-off occurred as a result of photo-excitation of electrons from valence band to conduction band. Incorporation of Cs^{3+} and Ni^{2+} ions increases the Urbach energy tail of the prepared samples which in turn courses a structural distortion in the crystal structure. The band gap energy of the prepared sample was found to increase with increase in Cs^{3+} and Ni^{2+} ions concentration. The band gap energy obtained were found to be in a semiconductor region. Also, the VSM analysis shows that the M_s and H_c values decrease with increase in Cs^{3+} and Ni^{2+} ions concentration. The observed decrease in M_s and H_c values is consistent with reported data in the literature. The values of R indicate that the prepared samples has a single domain with uniaxial anisotropy. Additionally, the values of both K and H_k decrease with increase in Cs^{3+} and Ni^{2+} ions concentration. These decreases justified that the prepared sample has anisotropic nature and softer to magnetize in the direction of easy axis. From the results obtained, we can concluded that the prepared samples can be used for core material in transformer, core material in power transmission, nanoantennas, data storage device and energy storage devices due to its unique characteristics such as band gap energy in the semiconductor region, high saturation magnetization and low coercivity as a result of doping of Cs^{3+} with Zn^{2+} in A-site and Ni^{2+} with Fe^{3+} in B-site.

REFERENCES

Akhtar, M. N., Javed, S., Ahmad, M., Sulong, A. B., & Khan, M. A. (2020). Sol gel derived MnTi doped Co2 W-type hexagonal ferrites: Structural, physical, spectral and magnetic evaluations. *Ceramics International*, *46*(6), 7842–7849. https://doi.org/10.1016/j.ceramint.2019.12.003

Almessiere, M. A., Güner, S., Slimani, Y., Baykal, A., Shirsath, S. E., Korkmaz, A. D., Badar, R., & Manikandan, A. (2022). Investigation on the structural , optical , and magnetic features of Dy 3 + and Y 3 + co-doped Mn 0 . 5 Zn 0 . 5 Fe 2 O 4 spinel ferrite nanoparticles. *Journal of Molecular Structure*, *1248*, 131412. https://doi.org/10.1016/j.molstruc.2021.131412

Alrebdi, T. A., Khalil Yahaya, I., Mohammed, J., Wudil, Y. S., Paray, A., Tchouank Tekou Carol, T., Hafeez, H. Y., & Srivastava, A. K. (2022). Phase structure refinement, electric modulus spectroscopy, Urbach energy analysis, and magnetic properties of Ce3+–Ni2+-substituted Y-type barium hexaferrites. *Materials Science and Engineering B: Solid-State Materials for Advanced Technology*, *280*(January), 115682. https://doi.org/10.1016/j.mseb.2022.115682

Ananth Kumar, R. T., Chithra Lekha, P., Sanjeeviraja, C., & Pathinettam Padiyan, D. (2014). Evolution of structural disorder using Raman spectra and Urbach energy in GeSe0.5S1.5thin films. *Journal of Non-Crystalline Solids*, *405*, 21–26. https://doi.org/10.1016/j.jnoncrysol.2014.08.029

Aslam, A., Morley, N. A., Amin, N., Arshad, M. I., Ajaz, M., Ali, A., Mahmood, K., Bibi, A., Iqbal, F., & Hussain, S. (2020). Study of structural, optical and electrical properties of La3+doped Mg0.25 Ni0.15 Cu0.25 Co0.35 Fe2-x Lax O4 spinel ferrites. *Physica B: Physics of Condensed Matter*, *602*, 412565. https://doi.org/10.1016/j.physb.2020.412565

Azhar, M., Shakir, I., & Farooq, M. (2020). Impact of rare earth Dy + 3 cations on the various parameters of nanocrystalline nickel spinel ferrite. *Journal of Materials Research and Technology*, *9*(3), 5313–5325. https://doi.org/10.1016/j.jmrt.2020.03.057

Debnath, S., Das, A., & Das, R. (2021). Effect of cobalt doping on structural parameters , cation distribution and magnetic properties of nickel ferrite nanocrystals. *Ceramics International*, *47*(12), 16467–16482. https://doi.org/10.1016/j.ceramint.2021.02.095

Debnath, S., & Das, R. (2020). Study of the optical properties of Zn doped Mn spinel ferrite nanocrystals shows multiple emission peaks in the visible range –a promising soft ferrite nanomaterial for deep blue LED. *Journal of Molecular Structure*, *1199*, 127044. https://doi.org/10.1016/j.molstruc.2019.127044

Ghorbani, H., Eshraghi, M., Dodaran, A. A. S., Kameli, P., Protasowicki, S., Johnson, C., & Vashaee, D. (2022). Effect of Yb doping on the structural and magnetic properties of cobalt ferrite nanoparticles. *Materials*

Research Bulletin, *147*(September 2021), 111642. https://doi.org/10.1016/j.materresbull.2021.111642

Hamza, M., Ali, I., Asif, M., & Ahmad, M. (2022). Detailed analysis of lanthanum impact on structural , morphological and magnetic properties of manganese spinel ferrites (MnLa x Fe 2-x O 4 x = (0 . 0 , 0 . 1 , 0 . 2) synthesized through hydrothermal techniq. *Journal of Magnetism and Magnetic Materials*, *564*(P1), 169852. https://doi.org/10.1016/j.jmmm.2022.169852

Kareemah A. L., Faiza A., Nasir, N. A. Yakubu A., and Fatima K. (2024) "Assessment of Radiation Dose Associated with Background Radionuclides in Quarry Soil at Dawakin-Kudu LGA Kano Nigeria. Nigerian Journal of Physics Volume 33(1). March 2024 http://doio.org/10.62292/njp.v33i1.2024.218

Kiran, A., Niaz, M., Yousaf, M., Mujassam, K., Aldossary, O. M., & Naeem, S. (2021). In fl uence of Y 3 þ , Yb 3 þ , Gd 3 þ cations on structural and electromagnetic properties of CuFe 2 O 4 nanoferrites prepared via one step sol-gel method. *Journal of Rare Earths*, *39*(10), 1224–1231. https://doi.org/10.1016/j.jre.2020.12.003

Manikandan, A., Kennedy, L. J., Bououdina, M., & Vijaya, J. J. (2014). Synthesis, optical and magnetic properties of pure and Co-doped ZnFe2O4 nanoparticles by microwave combustion method. *Journal of Magnetism and Magnetic Materials*, *349*, 249–258. https://doi.org/10.1016/j.jmmm.2013.09.013

Mohammed, J., Batoo, K. M., Abdulaziz, A. S., Safana, A. S., Hafeez, H. Y., Raslan, E. H., Hadi, M., Assiafan, A. A. K., Imran, A., & Srivastava, A. K. (2021). Crystal structure refinement and the magnetic and electro-optical properties of Er3+–Mn2+-substituted Y-type barium hexaferrites. *Ceramics International*, *47*(13), 18455–18465. https://doi.org/10.1016/j.ceramint.2021.03.169

Naik, S. R., Salker, A. V., Yusuf, S. M., & Meena, S. S. (2013). Influence of Co2+ distribution and spin-orbit coupling on the resultant magnetic properties of spinel cobalt ferrite nanocrystals. *Journal of Alloys and Compounds*, *566*, 54–61. https://doi.org/10.1016/j.jallcom.2013.02.163

Narang, S. B., & Pubby, K. (2021). Nickel Spinel Ferrites: A review. *Journal of Magnetism and Magnetic Materials*, *519*, 167163. https://doi.org/10.1016/j.jmmm.2020.167163

Nasir, S., Saleemi, A. S., & Anis-ur-rehman, M. (2013). Enhancement in dielectric and magnetic properties of Ni – Zn ferrites prepared by sol – gel method. *Journal of Alloys and Compounds*, *572*, 170–174. https://doi.org/10.1016/j.jallcom.2013.03.160

Niaz, M., Yousaf, M., Lu, Y., Azhar, M., Sarosh, A., Arshad, M., Niamat, M., Farhan, M., Ahmad, A., & Umar, M. (2021). Physical , structural , conductive and magneto-optical properties of rare earths (Yb , Gd) doped Ni – Zn spinel nanoferrites for data and energy storage devices. *Ceramics International*, *47*(9), 11878–11886. https://doi.org/10.1016/j.ceramint.2021.01.028

Pubby, K., Vijay Babu, K., & Bindra Narang, S. (2020). Magnetic, elastic, dielectric, microwave absorption and optical characterization of cobalt-substituted nickel spinel ferrites. *Materials Science and Engineering B: Solid-State Materials for Advanced Technology*, *255*(July 2018), 114513. https://doi.org/10.1016/j.mseb.2020.114513

Puli, V. S., Adireddy, S., & Ramana, C. V. (2015). Chemical bonding and magnetic properties of gadolinium (Gd) substituted cobalt ferrite. *Journal of Alloys and Compounds*, *644*, 470–475. https://doi.org/10.1016/j.jallcom.2015.05.031

Rahman, A., Zulfiqar, S., Ul, A., Alsafari, I. A., Yaqub, U., Farooq, M., & Shahid, M. (2021). Cd-Gd-doped nickel spinel ferrite nanoparticles and their nanocomposites with reduced graphene oxide for catalysis and antibacterial activity studies. *Ceramics International*, *47*(7PA), 9513–9521. https://doi.org/10.1016/j.ceramint.2020.12.085

Sandeep, A., Ganesh, G., Swathi, S., Rajesh, N., Sreelatha, M., N, P. K. K., Brahmanandam, B., Bose, S. C., Ravinder, D., Shanker, J., & Kumar, P. (2022). Synthesis , structural , magnetic and optical studies of Eu doped Ni – Zn nano ferrites. *Ceramics International*, *48*(19PB), 29493–29501. https://doi.org/10.1016/j.ceramint.2022.07.071

Shah, J., & Kotnala, R. K. (2012). Room temperature magnetoelectric coupling enhancement in Mg-substituted polycrystalline GdFeO 3. *Scripta Materialia*, *67*(4), 316–319. https://doi.org/10.1016/j.scriptamat.2012.05.003

Toprak, M. (2014). Cation distribution and magnetic properties of nanocrystalline gallium substituted cobalt ferrite. *Journal of Alloys and Compounds*, *615*, 181–187. https://doi.org/http://dx.doi.org/10.1016/j.jallcom.2014.06.156

Zan, F., Ma, Y., Ma, Q., Xu, Y., Dai, Z., Zheng, G., Wu, M., & Li, G. (2013). Magnetic and impedance properties of nanocomposite CoFe2 O 4/ Co0.7 Fe0.3 and single-phase CoFe 2 O4 prepared via a one-step hydrothermal synthesis. *Journal of the American Ceramic Society*, *96*(10), 3100–3107. https://doi.org/10.1111/jace.12437